



Spatial–Temporal Variability of Land Surface Temperature Spatial Pattern: Multifractal Detrended Fluctuation Analysis

Qin Nie , Kai Shi , Yi Gong, Feipeng Ran, Zongmei Li, Runjing Chen, and Lizhong Hua

Abstract—In order to investigate the spatial–temporal variability of land surface temperature (LST) spatial distribution in the context of rapid urbanization, we introduced the multifractal detrended fluctuation analysis (MFDFA) to the LST patterns in Xiamen city and Xiamen Island, China, during 1994–2015. Results reveal the almost same long-range dependence of the LST spatial pattern both in Xiamen city and Xiamen Island. LST has a long memory for a certain spatial range of LST values, such that a large increment in LST value is likely to be followed by a large increment in LST values of a certain spatial range. On the other hand, the LST spatial pattern possesses a multifractal nature, which shows an increasing trend over time as urbanization increased both in the whole study area and in the Xiamen Island. The irregularity of fractal structure exhibits a similar change from 1994 to 2015 in Xiamen city, as revealed by the multifractal spectrum with left-hook shapes. However, the multifractal spectrums exhibit different shapes for different study years in Xiamen Island, capturing the evolution from right-hook shape to left-hook shape and finally to a symmetrical shape. The difference in land surface change in small spatial scale leads to the variation in multifractal parameters. Meantime, differentiated from the previous study, we found that this long-range dependence is probably influenced by the natural factors, such as the local climate, atmospheric circulation, and any other factors.

Index Terms—Land surface temperature (LST), long-range dependence, multifractal detrended fluctuation analysis (MFDFA), Xiamen city.

I. INTRODUCTION

ALTHOUGH urbanized land currently covers only approximately 2% of global land area, more than half of the world’s population live in the urban environment [1]. Our world

Manuscript received March 12, 2020; revised April 17, 2020; accepted April 20, 2020. Date of publication April 28, 2020; date of current version May 21, 2020. This work was supported in part by the National Natural Science Foundation of China under Grants 41501447, 41804019, and 41471366, in part by the Science and Technology Planning Project of Xiamen, China, under Grant 3502Z20193059, and in part by the Natural Science Foundation of Fujian Province, China, under Grant 2018J01480. (Corresponding author: Kai Shi.)

Qin Nie, Feipeng Ran, Zongmei Li, and Lizhong Hua are with the Department of Spatial Information Science and Engineering, Xiamen University of Technology, Xiamen 361024, China (e-mail: nieqinhongyi@163.com; ran@xmut.edu.cn; lizongmei106@163.com; lzhua@xmut.edu.cn).

Kai Shi is with the College of Biology and Environmental Sciences, Jishou University, Jishou 416000, China (e-mail: einboplure@163.com).

Yi Gong is with Sustainable Places Research Institute, Cardiff University, Cardiff CF10 3BA, U.K. (e-mail: gongy2@cardiff.ac.uk).

Runjing Chen is with the Department of Surveying and Remote Sensing Engineering, Xiamen University of Technology, Xiamen 361024, China (e-mail: chenrunjing@163.com).

Digital Object Identifier 10.1109/JSTARS.2020.2990479

is urbanizing at an unprecedented speed. Urbanization transforms natural vegetation and water covers to anthropogenic land coverage [2]. It has been confirmed that these conversions affect regional climate and cause climatologically phenomenon—urban heat island effect (UHI), which leads to many negative effects, such as increasing thermal discomfort, raising energy consumption, and air pollution [3]–[5]. Consequently, the causes and impacts of UHI and their qualitative and quantitative characteristics have attracted increasing interest [6]–[10].

Satellite remote sensing provides the only viable option to detect and monitor UHI from space in an efficient, affordable, and timely manner. In recent decades, land surface temperature (LST) derived from remote sensing data has been widely utilized to analyze UHI characteristics, climate modeling, and global-change monitoring studies on regional and global spatial scale [11]–[13]. LST is one of the primary parameters controlling the physical, chemical, and biological processes of the earth. A large number of studies [14]–[17] have focused on the relationship between LST and land use/cover and urban surface biophysical composition, which contributes the understanding of the effects of urbanization on UHI.

Although the correlation mentioned above has been studied in connection with the increase in urbanization level, analyzing and understanding how LST has been varying in spatial and temporal dimensions is a prerequisite for these related studies. However, the existing studies on LST dynamic mainly focused on the depiction and quantitative temporal comparison of LST spatial distribution or LST time series analysis over time [18]. This is not sufficient for quantitative measurement of LST pattern. Developing new methods to effectively analyze LST spatio-temporal variability is an important issue.

In fact, LST dynamic is a coupled natural–human–social–economic–geographical complex system, which may seem fragmented and random, but they are geographical complexities with self-similar characteristics. Furthermore, the spatial–temporal variation of LST pattern is a complex question with both spatial autocorrelation and spatial heterogeneity. LST patterns have an extremely wide range of spatio-temporal scales, necessitating the application of fractal theory into the analyses.

Fractal geometry, as one of the main methods of understanding complexity, can characterize the rational mechanism of LST patterns. There have been many studies on fractal characters of temperature time series. For example, Jiang *et al.* [19] analyzed multifractal phenomena of the daily air temperature and the

surface temperature over China. However, 2-D fractal characteristic has been rarely studied, especially for LST spatial pattern [20].

The long-range power-law correlations have been discovered in a remarkably wide variety of systems [21]. The detrended fluctuation analysis (DFA) method has been introduced to qualify scaling behaviors in many fields, invented by Peng *et al.*, [22] to investigate the long-range dependence in coding and noncoding DNA nucleotide sequence. Then, it was generalized to study the multifractal nature hidden in time series [23], termed multifractal DFA (MFDFA), which has been widely used in various studies [24]. Gu and Zhou [25] successfully generalized the 1-D DFA and MFDFA to a 2-D framework. Then, the 2-D MFDFA has been applied widely, yielding correct results for a 2-D array and more in-depth information [26]–[28]. Niu *et al.* [29] applied MFDFA to confirm the multifractal nature of the flame images. Liu *et al.* [30] employed the MFDFA to reveal the multifractal properties of the fracture surfaces of foamed polypropylene/polyethylene blends at different temperatures. Yadav *et al.* [31] employed it to characterize the LiF thin-film morphologies. It has been recently realized that MFDFA can be used not only to characterize the surface morphologies, but also to reveal the long-range dependence of surfaces in 2-D.

The present study introduces 2-D MFDFA to LST spatial patterns in the rapidly urbanizing subtropical city of Xiamen, China, for a 21-year period from 1994 to 2015. LST spatial distribution is first retrieved from Landsat TM/OLI/TIRS images during 1994–2015 by the monowindow algorithm. The specific objectives are

- 1) to investigate and compare the long-range dependencies in the LST spatial pattern of Xiamen city and Xiamen Island;
- 2) to reveal and compare the multifractal features in the LST pattern of Xiamen city and Xiamen Island; and
- 3) to explore the practical meaning of the multifractal parameters.

II. METHODOLOGY

A. Study Area and Image Data

This study focuses on Xiamen city, a subtropical coastal city in Fujian province, southeastern China. Since the early 1980s when China began its economic reform, as one of the four earliest established special economic zones in China, Xiamen has been undergoing accelerated economic growth, urbanization, industrial expansion, and population growth. With the development of urbanization, it has been suffered from a degree of uncomfortably hot in summer. It is expected to experience further dramatic urbanization for the foreseeable future. The city comprises Xiamen Island of two districts (Siming and Huli) and four surrounding districts: Jimei, Haicang, Tong'an, and Xiang'an (see Fig. 1). As the urban nucleus and the biggest island in Xiamen city, Xiamen Island covers 158 km², accounting for about 9.3% of the Xiamen city's area, but its population is about 1.152 million (2018), accounting for 55.4% of the city's registered population. With the development of urbanization, LST spatio-temporal patterns present many differences between the both areas.

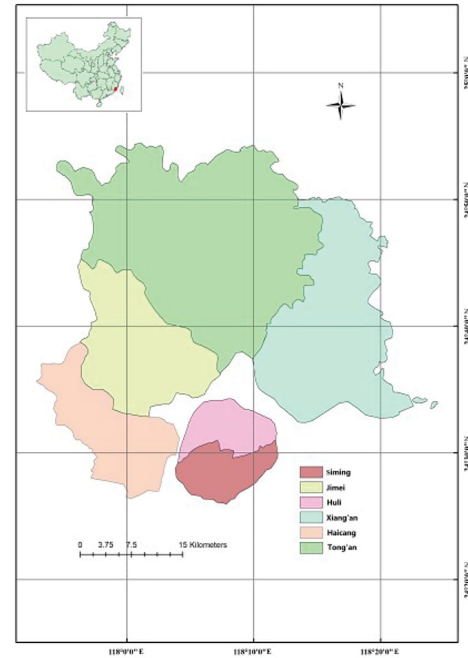


Fig. 1. Map of the Xiamen study area.

Five cloud-free Landsat TM/OLI/TIRS images that cover a 21-year period (acquired in 1994, 2000, 2004, 2010, and 2015) were selected as the primary data for mapping LSTs in the study area. The MODTRAN4-based FLAASH module of the ENVI4.7 software is adopted to remove atmospheric influence. An image-to-image registration among the five images was carried out using a second-order polynomial transformation and nearest neighbor resampling. The overall root mean square error values are less than 15 m (0.5 pixels).

B. LST Derived

The Landsat thermal band was employed to derive LST. The digital number (DN) of the raw images is first converted to at-satellite spectral radiance (L_λ) as follows:

$$L_\lambda = \text{gain} \times \text{DN} + \text{offset} \quad (1)$$

where $gain$ is the slope of the conversion function, and $offset$ is the intercept of the conversion function, which are supplied in the metadata of each TM/OLI/TIRS image.

The effective at-satellite temperature (T_B) can then be obtained from spectral radiance using the following equation under an assumption of unity emissivity [32]:

$$T_B = \frac{K_2}{\ln\left(\frac{K_1}{L_\lambda} + 1\right)} \quad (2)$$

where K_1 and K_2 are calibration constants supplied in the metadata of the Landsat images. To obtain LST, T_B has to be corrected with emissivity (ε) as follows [33]:

$$\text{LST} = \frac{T_B}{1 + \left(\lambda \times \frac{T_B}{\rho}\right) \ln \varepsilon} \quad (3)$$

$$\rho = h \times \frac{c}{\sigma} \quad (4)$$

where λ is the wavelength of the emitted radiance ($11.5 \mu\text{m}$), h is Planck's constant (6.626×10^{-34} Js), σ is the Boltzmann constant (1.38×10^{-23} J/K), and c is the velocity of light (2.998×10^8 m/s). We use the normalized difference vegetation index (NDVI) threshold method to obtain the parameter ε . Van de Griend [34] reported that thermal emissivity ε is highly correlated with NDVI after logarithmic transformation (correlation coefficient of $R^2 = 0.9$) and proposed the following empirical relationship:

$$\varepsilon = 1.0094 + 0.047 \ln(\text{NDVI}). \quad (5)$$

This formula is suitable when the NDVI is greater than 0.157. According to Gong *et al.* [35], a land surface thermal emissivity value of 0.923 is appropriate for land surfaces where the NDVI is less than 0.157, and a value of 0.9925 is suitable for water body thermal emissivity.

C. Multifractal Detrended Fluctuation Analysis

MF DFA were employed to explore the long-range dependence and multifractal nature of LST spatial pattern, which can be referred to the original source [25] for a detailed description of the method. MF DFA has been widely used in various studies [31].

Consider a 2-D surface that is denoted by array $X(i, j)$, $i = 1, 2, \dots, M$ and $j = 1, 2, \dots, N$, the surface $X(i, j)$ is partitioned into $M_s \times N_s$ ($M_s = \lfloor M/s \rfloor$, $N_s = \lfloor N/s \rfloor$) disjoint square segments of the same size $s \times s$. Each segment can be denoted by $X_{v,w}(i, j) = X(l_1 + i, l_2 + j)$, $1 \leq i, j \leq s$, $l_1 = (v-1)s$, and $l_2 = (w-1)s$. The cumulative sum $u_{v,w}(i, j)$ is calculated as follows:

$$u_{v,w}(i, j) = \sum_{k_1=1}^i \sum_{k_2=1}^j X_{v,w}(k_1, k_2) \quad (6)$$

where $1 \leq i, j \leq s$.

The trend of the cumulative sum, $\tilde{u}_{v,w}$, can be determined by fitting it with the least square method. The residual matrix can be obtained as

$$\epsilon_{v,w}(i, j) = u_{v,w}(i, j) - \tilde{u}_{v,w}(i, j). \quad (7)$$

The detrended fluctuation function of the segment $X_{v,w}$ is defined as follows:

$$F^2(v, w, s) = \frac{1}{s^2} \sum_{i=1}^s \sum_{j=1}^s \epsilon_{v,w}(i, j)^2. \quad (8)$$

The overall detrended fluctuation is calculated by averaging over all the segments

$$F_q(s) = \left\{ \frac{1}{M_s N_s} \sum_{v=1}^{M_s} \sum_{w=1}^{N_s} [F(v, w, s)]^q \right\}^{1/q} \quad (9)$$

where q can take any real value except for $q = 0$.

When $q = 0$

$$F_0(s) = \exp \left\{ \frac{1}{M_s N_s} \sum_{v=1}^{M_s} \sum_{w=1}^{N_s} \ln [F(v, w, s)] \right\}. \quad (10)$$

TABLE I
STATISTICS OF MULTIFRACTAL PARAMETERS IN XIAMEN CITY
FROM 1994 TO 2015

	a_{\min}	a_{\max}	$\Delta\alpha$	Δh	$f(a_{\min})$	$f(a_{\max})$	Δf	$h(q=2)$
1994	1.884	2.42	0.535	0.393	1.066	0.093	0.973	1.021
2000	1.85	2.533	0.682	0.513	0.706	-0.088	0.794	1.039
2004	1.869	2.477	0.607	0.457	0.988	0.012	0.976	1.02
2010	1.783	2.495	0.711	0.545	0.631	0.048	0.583	1.006
2015	1.857	2.476	0.619	0.464	0.863	0.031	0.832	1.025

Varying the value of s , the scaling relation between the detrended fluctuation function $F(s)$ and the scale s can be obtained

$$F_q(s) \sim s^{2h(q)} \quad (11)$$

where $h(q)$ is the generalized Hurst exponent. The scaling exponent $h(q)$ is a nonlinear decreasing function of q for multifractals. The $h(q)$ represents the effect of different levels of fluctuations on the function $F_q(s)$, describing the scaling behavior of small fluctuations in the LST pattern when $q < 0$ and that of large fluctuations when $q > 0$. As $q = 2$, $h(2)$ is the Hurst index, describing the long-range dependence of the LST pattern. It quantifies the relative tendency of LST spatial distribution either to regress strongly to the mean or to cluster in a direction. The mass exponent $\tau(q)$ can be obtained as

$$\tau(q) = qh(q) - D_f \quad (12)$$

where D_f is the fractal dimension of the geometric support of the multifractal measure.

Finally, the singularity strength function $a(q)$ and the singularity spectrum $f(a)$ may be determined using Legendre's transformation [36]

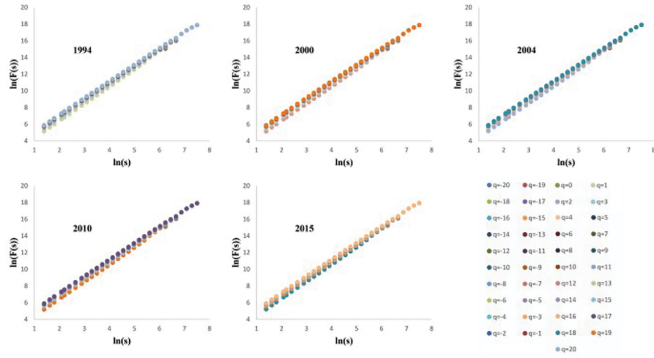
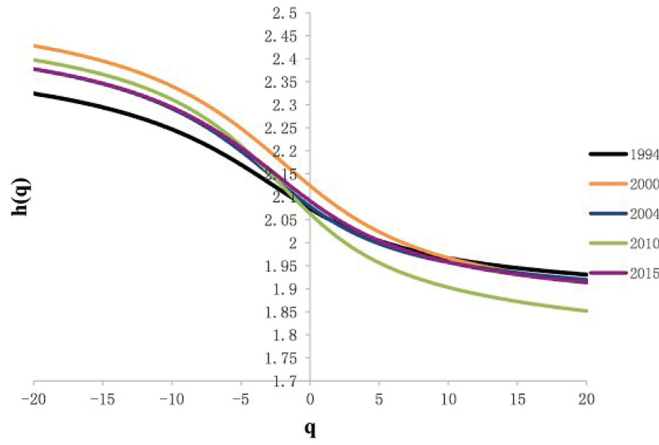
$$a(q) = \frac{d\tau(q)}{dq} \quad \text{and} \quad f(a) = qa(q) - \tau(q) \quad (13)$$

where a is singularity exponent, describing the irregularity of different fluctuation measures in the LST spatial pattern, and $f(a)$ is the fractal dimension under the specific singularity index. The curve $a \sim f(a)$ constitutes the multifractal spectrum. The shape and extension of $f(a)$ curve contain significant information about the LST spatial distribution. The spectrum width is defined as $\Delta a = a_{\max} - a_{\min}$, where a_{\min} and a_{\max} mean the singularity of maximum and minimum fluctuation measures, respectively. The parameter Δa has been identified as the degree of multifractality for singularity exponent.

III. RESULTS

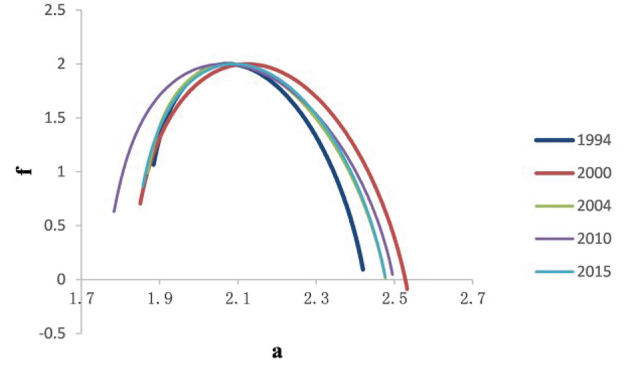
A. MF DFA on LST Spatial Pattern in Xiamen City

The MF DFA is applied to obtain the scaling properties of LST images for the study period of 1994–2015. As listed in Table I, all the $h(2)$ values are larger than 0.5, implying that there is a strong positive long-range correlation in the LST pattern during the study years. The long-range correlation property signifies that LST fluctuations in small spatial intervals are


 Fig. 2. $\ln(s) \sim \ln(F_q(s))$ graphs in Xiamen city during 1994–2015.

 Fig. 3. Generalized Hurst exponents $h(q)$ for q in Xiamen city.

positively correlated to fluctuations in larger spatial intervals. This long-range dependence refers to the “long memory” or internal correlation within the spatial LST pattern. In other word, an increase (decrease) in the LST value will result in an increase (decrease) in LST values of a different spatial scale. This finding also suggests that the correlations between the LST fluctuations do not obey the classical Markov-type stochastic behavior (exponential decrease with space), but rather decay with space in a slower fashion.

Next, q - $h(q)$ curve is applied to check whether the LST spatial pattern possesses a multifractal nature. The scaling relations between the detrended fluctuation function $F(s)$ and the scale s for different q are shown in Fig. 2. The data points for every q fall on a straight line, indicating a perfect power-law scaling between $F(s)$ and s , from which the generalized Hurst exponent $h(q)$ can be obtained. As illustrated in Fig. 3, the $h(q)$ exhibits a nonlinear relationship with q for all the study years, highlighting the evident multifractal behavior in the LST pattern. A series of scaling exponent are required to disclose the LST spatial patterns. The width of $h(q)$ curve ($\Delta h(q) = h(q)_{\max} - h(q)_{\min}$) shows a measure of the multifractality and indicates the deviation from monofractal behavior. A fluctuated increasing trend of Δh values has been presented during the study period, suggesting the increasing multifractality on the whole from 1994 to 2015. The $h(q < 0)$ describes the scaling behavior of small fluctuations in the LST pattern, and $h(q > 0)$


 Fig. 4. $a \sim f(a)$ graphs in Xiamen city during 1994–2015.

denotes that of large fluctuations. The curves of $h(q < 0)$ are scattered from 1994 to 2015. Conversely, $h(q > 0)$ gather together except that of 2010. All those suggest that the scaling behavior of small fluctuations varied larger. It is also observed that the large fluctuations (positive q) appear to have smaller values of $h(q)$ than the small fluctuations. This is the usual case for multifractal series.

The singularity exponent a describes the irregularity of different fluctuation measures in the LST spatial pattern. From Table I, we can see that a_{\min} varies from 1.783 to 1.884, with little change. However, a_{\max} is between 2.42 and 2.533, exhibiting an increase from 1994 to 2015 on the whole. The width $\Delta a = a_{\max} - a_{\min}$ describes the range of fluctuation measures. The greater the value, the wider the fluctuation distribution and the more irregular the fluctuation in the LST spatial pattern. An increase in Δa is observed from 1994 to 2015 on the whole, with values between 0.535 and 0.711, indicating an increased multifractality in the fluctuation of LST.

Fig. 4 shows the multifractal spectrum in Xiamen city from 1994 to 2015. In all cases, the spectrum has a left truncation and a long right tail, suggesting the similar change in the irregularity of fractal structure. The $f(a)$ reaches to the maximum as $q = 0$, whereas $f(a)$ on the left of the maximum correspond to $q > 0$ and $f(a)$ on the right of the maximum correspond to $q < 0$. It can be seen that $f(a)$ fluctuates more significantly at the side of $q < 0$ comparing with that at $q > 0$. This is attributed to the spatial multifractal structure that is insensitive to the local fluctuations with large magnitudes.

Multifractal analysis can describe the different fluctuations in the LST spatial pattern by a series of fractal dimensions. The $f(a_{\max})$ reflects the fractal dimension of the subset of minimum fluctuation, and the $f(a_{\min})$ reflects that of the maximum fluctuation. Thus, the $\Delta f(a) = f(a_{\min}) - f(a_{\max})$ can describe the ratio between the regions where the fluctuation measure distributes most maximum and most minimum. Positive Δf means that the dataset is dominated by local fluctuations with large magnitudes. As listed in Table I, the Δf was all positive, indicating that local fluctuations with large magnitudes were dominant during all the study period.

B. MF DFA on LST Spatial Pattern in Xiamen Island

Xiamen Island is the urban nucleus of Xiamen city, comprising two districts, namely Siming and Huli. It is the earliest

TABLE II
STATISTICS OF MULTIFRACTAL PARAMETERS IN XIAMEN ISLAND
FROM 1994 TO 2015

	a_{\min}	a_{\max}	$\Delta\alpha$	Δh	$f(a_{\min})$	$f(a_{\max})$	Δf	$h(q=2)$
1994	1.979	2.054	0.075	0.056	1.751	1.855	-0.104	1.008
2000	1.962	2.092	0.13	0.103	1.696	1.771	-0.075	1.008
2004	1.98	2.069	0.089	0.068	1.735	1.838	-0.103	1.01
2010	1.977	2.108	0.131	0.092	1.719	1.497	0.222	1.011
2015	1.985	2.109	0.123	0.104	1.803	1.808	-0.005	1.012

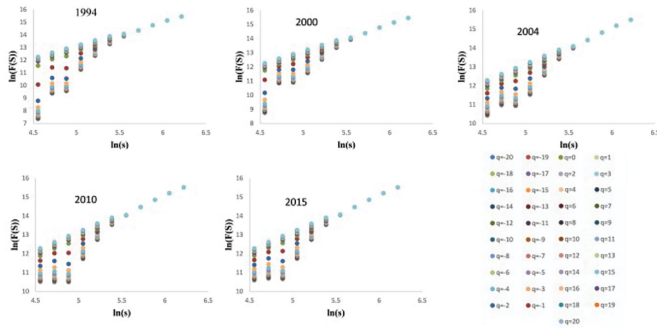


Fig. 5. $\ln(s) \sim \ln(F_q(s))$ graphs in Xiamen Island during 1994–2015.

urbanized area since the economic reforms of the early 1980s and has witnessed rapid urban growth. Consequently, like many hot subtropical cities, Xiamen Island suffers from a degree of thermal discomfort in summer. In the following, the MFDFA was applied to LST spatial distribution in Xiamen Island from 1994 to 2015.

As listed in Table II, all the $h(2)$ values are greater than 0.5, indicating that LST distribution has a positive long-range correlation in Xiamen Island, that is, the LST fluctuation is not a random process, and there is a consistent change trend within a certain scale (all increasing or decreasing). Fig. 5 shows the log–log plots of $F_q(s)$ versus s for q varying from -20 to 20 in all the study years. From these plots, we can see that the linear relationship can fit the curve of fluctuation functions well for each q . This indicates that there exists a power-law function relation between $F_q(s)$ and q . Fig. 6 shows the generalized Hurst exponents $h(q)$ with varying moments q , respectively. The exponents $h(q)$ decrease with the increase in the moment q , which indicates the presence of the strong multifractal behavior in the LST spatial pattern. The Δh values can be used to describe the multifractality. We observe the increasing multifractality for LST spatial distribution from 1994 to 2015, indicated by the increasing Δh values (see Table II). Specifically, the scaling behavior of the fluctuation subset with small magnitudes varied large, indicated by the scatter curves of $h(q < 0)$ from 1994 to 2015, however, that with large magnitudes varied little by the gathered curves of $h(q > 0)$ throughout the study period.

As listed in Table II, both parameters a_{\min} and a_{\max} are increased on the whole from 1994 to 2015, ranging from 1.962 to 1.985 and from 2.054 to 2.109, respectively, indicating the increased singularity of maximum and minimum fluctuation measures. Correspondingly, the width Δa is observed to

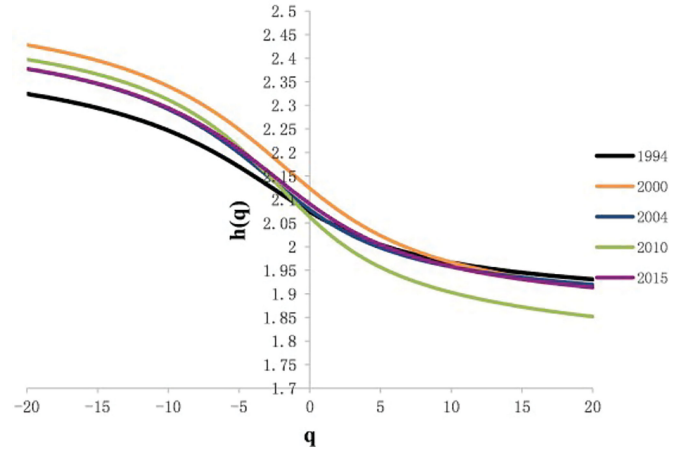


Fig. 6. $q \sim h(q)$ graphs from 1994 to 2015 in Xiamen Island.

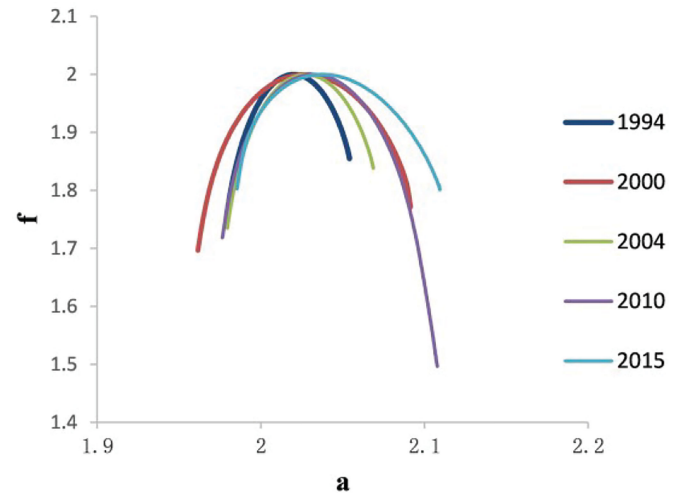


Fig. 7. $a \sim f(a)$ graphs in Xiamen Island during 1994–2015.

increase during the study period, with values between 0.075 and 0.13, which suggests an increased multifractality and spatial heterogeneity in the LST fluctuation.

The shape and width of multifractal spectrum show the multifractal nature of LST fluctuation subset of different magnitudes. Multifractal spectrum $f(a)$ is shown in Fig. 7. The multifractal spectrums exhibit different shapes for different study years. During the period of 1994–2004, it has shapes of right-hook, and all the curves fluctuates more significantly at the side of $q > 0$, indicating that the spatial multifractal structure is sensitive to the local fluctuations with large magnitudes. Conversely, the $f(a)$ exhibits shape of left-hook in 2010, and it fluctuates more significantly at the side of $q < 0$. In 2015, the $f(a)$ exhibits symmetrical shape. On the other hand, the width of multifractal spectrum, $\Delta f(a)$, is negative from 1994 to 2004, which suggests that the frequency of the small fluctuation subset is larger than that of the large fluctuation measure, and the LST data fluctuation is more concentrated in the small fluctuation. In 2010, the Δf is positive, indicating that local fluctuations with large magnitudes were dominant in this year. It is about zero in 2015, showing

the equal frequency distribution between the small fluctuation subset and the large ones.

IV. DISCUSSION AND CONCLUSION

A. Long-Range Dependence in LST Spatial-Temporal Variation

LST is a key parameter for the Earth's energy budget. Understanding the spatial distribution and dynamic change in LST is essential to monitor the energy balance and climate change of the Earth. The long-range dependence suggests that an increase (decrease) in a physical variable will result in an increase (decrease) in the physical variable of a different spatial scale, which implies a self-similarity in the spatial variability of physical elements. The existence of long-range correlation in the LST pattern can help evaluating urban environment and modeling urban climate.

Urban thermal environment field is a nonlinear, nonequilibrium, complex adaptive system. The spatial pattern and differentiation of LST may seem fragmented and random, but they are geographical complexities with self-similar characteristics. A series of scaling exponent are required to disclose the long-range correlation in LST spatial patterns. The singularity exponent a describes the irregularity of different fluctuation measures, in which a can be used to locate different magnitudes of fluctuation in the LST spatial pattern. This can provide references for information recognition and extraction from thermal field and thermal interpolation.

The almost same long-range dependence of LST spatial distribution has been uncovered for Xiamen city and Xiamen Island throughout the study period from Section III, indicated by the little difference in $h(2)$. What factors have led to the similar LST long-range dependence? Many previous studies have shown that the LST pattern is strongly related to surface properties [3], [14]–[17]. Urban thermal field is directly affected by the complex land surface pattern and their thermal environment process. We mapped the land use/cover change (LUCC) over the study period using the maximum likelihood procedure, and four types of LUCC (forest, cultivated, construction, and unutilized) have been identified (see Fig. 8). Spatially, Xiamen has experienced dramatic land use changes since the 1990s. It has been transformed from an island city to a bay-like city during the study period. Among the four LUCC types, construction land increased most rapidly, from 137.5 km² in 1994 to 469.6 km² in 2015, which represents a 2.4-fold increase over the past 21 years, which was at the expense of the other land types. The cultivated land declined most rapidly, from 36.8% to 24.1% of the study area. Lin *et al.* [37] also found the large-scale land surface change in Xiamen city. From 1995 to 2004, the urban area of Xiamen Island increased from 58.90 to 85.10 km². More than half of the water area and one third of coastal wetland were converted into urban areas. From 2004 to 2007, farmland and coastal wetland became reduced by 37% and 39%, respectively, as a result of urban sprawl. Many other research works [38], [39] also report similar conclusions. Therefore, it can be concluded that LUCC is not the dominant factor controlling the similar long-range dependence of LST spatial patterns during the study period.

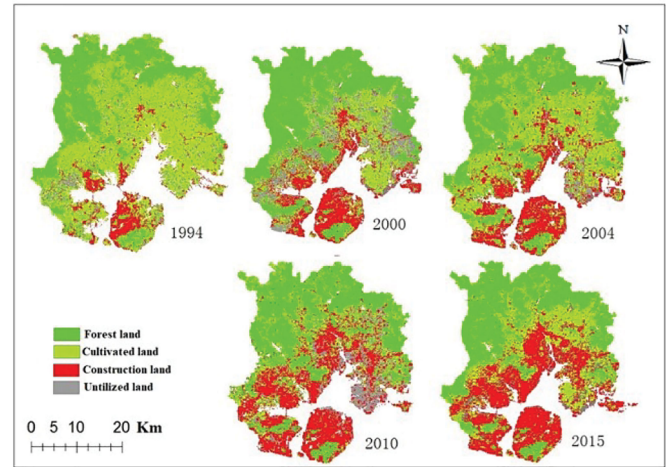


Fig. 8. LUCC in Xiamen during 1994–2015.

LST is the result of a combination of natural factors (such as rainfall, atmospheric circulation, and wind speed) and nonnatural factors (such as impervious surface (IS), population, and energy consumption). Xiamen is situated in subtropical Asian monsoon system in the coast area of Southeastern China, where the annual temperature, relative humidity, rainfall, and wind speed are 21.4 °C, 82%, 2168.2 mm, and 2.7 m/s, respectively. Therefore, LST in Xiamen differs from that of inland cities as a result of the influence of, and modification by, the nearby sea. Climate factors, especially sea-land wind, have a significant mitigating effect on the urban heat island. We can conclude that the natural factors, such as the local climate and atmospheric circulation, and any other factors control the similar long-range dependence of LST spatial patterns during the study period.

B. Practical Meaning of Multifractal Parameters in LST Spatial-Temporal Variation

Different from the similar LST long-range dependence, it can be seen obviously that there are many differences in multifractal parameters between Xiamen city and Xiamen Island. The multifractality of Xiamen Island indicated by Δa is much smaller than that of Xiamen city during the study period; the spatial multifractal structure $f(a)$ for Xiamen city is insensitive to the local fluctuations with large magnitudes, and local fluctuations with large magnitudes were dominant during all the study periods; however, some differences have been presented for Xiamen Island. During the period 1994–2004, the spatial multifractal structure is sensitive to the local fluctuations with large magnitudes, and the LST data fluctuation is more concentrated in the small fluctuation. They are conversely in 2010 and 2015, and the equal frequency distribution between the small fluctuation subset and the large ones is presented. All these multifractal parameters show the local differences of LST patterns during the urbanization process of Xiamen city.

The large-scale urban land surface change, such as the increasing of IS, determines the variation in multifractal parameters. As a Special Economic Zone, Xiamen city planning had become the most influential tool in guiding urban spatial development,

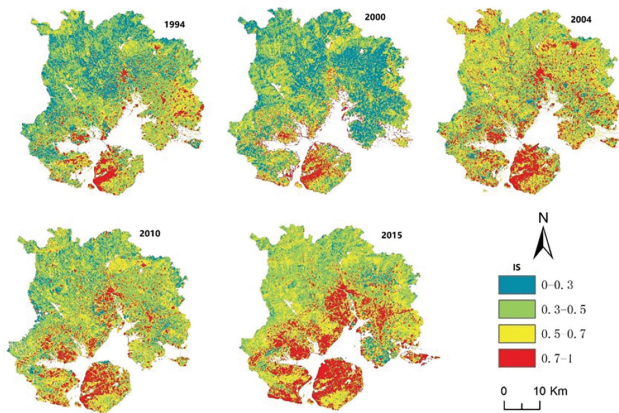


Fig. 9. IS maps in Xiamen from 1994 to 2015.

resulting in increasing of IS. IS has been widely utilized to quantify urban expansion and assess environmental impacts of urbanization [2]. We mapped IS spatial distribution by linear spectral mixture analysis. From Fig. 9, it is obvious that the IS spatial pattern expanded gradually along the bay during the study period, eventually matching the coastline. Xiamen Island, the city's main urban core, is the earliest urbanized area of Xiamen city and IS began to increase on the west of Xiamen Island since 1990s. From 1987 to 1995, the urban area of Xiamen Island nearly doubled in size and kept increasing to 85.10 km² in 2004 [37]. It reached saturation during 2004–2007. Since 2010, built-up land (IS greater than 0.7) has become the dominant landscape type in Xiamen Island. All these made the smaller LST multifractality of Xiamen Island than Xiamen city. To mitigate urban problems, the policy of expanding the urban space outside the island was put forward, and Xiamen has entered to the construction stage of gulf city. IS has grown rapidly outside of Xiamen island. According to image statistics, the area of IS (greater than 0.7) has increased from 144.07 km² in 1994 to 347.8 km² in 2015 by more than 2.4 times. Also, we calculated IS trajectories to reveal its spatio-temporal variation progression during the study period of 1994–2015. 20.96% of the study area have transformed into build-up land [40]. Spatially, the IS grow along the gulf, and the gulf-type IS pattern has been gradually appeared from 1994 to 2015.

C. Conclusion

The MFDFA shows that the LST spatial pattern exhibits similar long-range dependence for Xiamen city and Xiamen Island during the study period of 1994–2015. An increase (decrease) in the LST value will result in an increase (decrease) in LST values of a different spatial scales. LST is the result of a combination of natural factors (such as rainfall, atmospheric circulation, and wind speed) and nonnatural factors (such as IS, population and energy consumption). The natural factors, such as the local climate, atmospheric circulation, and any other factors, control the similar long-range dependence of LST spatial patterns during the study period.

The nonlinear relationship between $h(q)$ and q highlights the multifractality in the LST distribution. The multifractality of Xiamen Island is much smaller than that of Xiamen city.

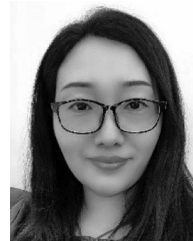
For Xiamen city, the multifractal spectrums present similar left-hook shapes from 1994 to 2015, and local fluctuations with large magnitudes are dominant during all the study periods. However, the multifractal spectrums exhibit different shapes for different study years in Xiamen Island, from shapes of right-hook during the period of 1994–2004 to left-hook shape in 2010 and a symmetrical shape in 2015. LST data fluctuation is more concentrated in the small fluctuation from 1994 to 2004, and local fluctuations with large magnitudes were dominant in 2010. Up to 2015, the frequency distribution between the small fluctuation subset and the large ones is uniform. All these multifractal parameters suggest how the spatial heterogeneity of the LST pattern varied with urbanization throughout the study period. The land surface change results in the differences of these multifractal parameters.

Many studies focus on the scale issue of UHI that exhibits different characteristics and patterns on different times and spatial scales. We introduce MFDFA into the LST spatio-temporal variability for the first time. Once the long-range dependence and multifractality in spatial–temporal dynamics of LST are understood, the formation mechanism of UHI can be explored better, and a wide range of strategies to reduce regional thermal environment can be applied to urban planning. This would facilitate the development of regional urban planning strategies to minimize local temperature rise and improve quality of life in future urban growth.

REFERENCES

- [1] Q. H. Weng, *Remote Sensing for Urbanization in Tropical and Subtropical Regions—Why and What Matters?* Boca Raton, FL, USA: CRC Press/Taylor & Francis, 2015.
- [2] Q. Nie, W. Man, Z. M. Li, and Y. T. Huang, "Spatiotemporal impact of urban impervious surface on land surface temperature in Shanghai, China," *Can. J. Remote Sens.*, vol. 42, no. 6, pp. 680–689, 2016.
- [3] H. Xu, D. Lin, and F. Tang, "The impact of impervious surface development on land surface temperature in a subtropical city: Xiamen, China," *Int. J. Climatol.*, vol. 33, no. 8, pp. 1873–1883, 2013.
- [4] M. L. Imhoff, P. Zhang, R. E. Wolfe, and L. Bounoua, "Remote sensing of the urban heat island effect across biomes in the continental USA," *Remote Sens. Environ.*, vol. 114, no. 3, pp. 504–513, 2010.
- [5] N. B. Grimm *et al.*, "Global change and the ecology of cities," *Science*, vol. 319, no. 5864, pp. 756–760, 2008.
- [6] M. Nastran, M. Kobal, and K. Eler, "Urban heat islands in relation to green land use in European cities," *Urban Forestry Urban Greening*, vol. 37, pp. 33–41, 2019.
- [7] R. Sun, Y. Lü, X. Yang, and L. Chen, "Understanding the variability of urban heat islands from local background climate and urbanization," *J. Cleaner Prod.*, vol. 208, pp. 743–752, 2019.
- [8] N. Shirani-Bidabadi, T. Nasrabadi, S. Faryadi, A. Larijani, and M. S. Roodposhti, "Evaluating the spatial distribution and the intensity of urban heat island using remote sensing, case study of Isfahan city in Iran," *Sustain. Cities Soc.*, vol. 45, pp. 686–692, 2019.
- [9] R. Yao, L. Wang, X. Huang, W. Zhang, J. Li, and Z. Niu, "Interannual variations in surface urban heat island intensity and associated drivers in China," *J. Environ. Manage.*, vol. 222, pp. 86–94, 2018.
- [10] J. Lai *et al.*, "Identification of typical diurnal patterns for clear-sky climatology of surface urban heat islands," *Remote Sens. Environ.*, vol. 217, pp. 203–220, 2018.
- [11] B. K. Bhattacharya, K. Mallick, N. K. Patel, and J. S. Parihar, "Regional clear sky evapotranspiration over agricultural land using remote sensing data from Indian geostationary meteorological satellite," *J. Hydrol.*, vol. 387, no. 1/2, pp. 65–80, 2010.
- [12] S. Fall, D. Niyogi, A. Gluhovsky, R. A. Pielke Sr, E. Kalnay, and G. Rochon, "Impacts of land use land cover on temperature trends over the continental United States: Assessment using the North American regional reanalysis," *Int. J. Climatol.*, vol. 30, no. 13, pp. 1980–1993, 2010.

- [13] V. Lakshmi, S. Hong, E. E. Small, and F. Chen, “The influence of the land surface on hydrometeorology and ecology: New advances from modeling and satellite remote sensing,” *Hydrol. Res.*, vol. 42, no. 2/3, pp. 95–112, 2011.
- [14] A. Mathew, S. Khandelwal, and N. Kaul, “Spatial and temporal variations of urban heat island effect and the effect of percentage impervious surface area and elevation on land surface temperature: Study of Chandigarh city, India,” *Sustain. Cities Soc.*, vol. 26, pp. 264–277, 2016.
- [15] Y. Zhang and L. Sun, “Spatial-temporal impacts of urban land use land cover on land surface temperature: Case studies of two Canadian urban areas,” *Int. J. Appl. Earth Observ. Geoinf.*, vol. 75, pp. 171–181, 2019.
- [16] J. Wang, Z. Qingming, H. Guo, and Z. Jin, “Characterizing the spatial dynamics of land surface temperature–impervious surface fraction relationship,” *Int. J. Appl. Earth Observ. Geoinf.*, vol. 45, pp. 55–65, 2016.
- [17] H. Fathizad, M. Tazeh, S. Kalantari, and S. Shojaei, “The investigation of spatiotemporal variations of land surface temperature based on land use changes using NDVI in southwest of Iran,” *J. Afr. Earth Sci.*, vol. 134, pp. 249–256, 2017.
- [18] Y. Liu, J. Peng, and Y. Wang, “Efficiency of landscape metrics characterizing urban land surface temperature,” *Landscape Urban Planning*, vol. 180, pp. 36–53, 2018.
- [19] L. Jiang, J. Zhang, X. Liu, and F. Li, “Multi-fractal scaling comparison of the air temperature and the surface temperature over China,” *Phys. A, Statist. Mech. Appl.*, vol. 462, pp. 783–792, 2016.
- [20] M. Das and S. K. Ghosh, “Short-term prediction of land surface temperature using multifractal detrended fluctuation analysis,” in *Proc. IEEE India Conf.*, pp. 1–6, 2014.
- [21] H. E. Stanley *et al.*, “Statistical mechanics in biology: How ubiquitous are long-range correlations?” *Phys. A, Statist. Mech. Appl.*, vol. 205, pp. 214–253, 1994.
- [22] C. K. Peng, S. V. Buldyrev, S. Havlin, M. Simons, H. E. Stanley, and A. L. Goldberger, “Mosaic organization of DNA nucleotides,” *Phys. Rev. E*, vol. 49, no. 2, pp. 1685, 1994.
- [23] J. W. Kantelhardt, S. A. Zschiegner, E. Koscielny-Bunde, S. Havlin, A. Bunde, and H. E. Stanley, “Multifractal detrended fluctuation analysis of nonstationary time series,” *Phys. A, Statist. Mech. Appl.*, vol. 316, pp. 87–114, 2002.
- [24] K. Chanda, S. Shet, B. Chakraborty, A. K. Saran, W. Fernandes, and G. Latha, “Fish sound characterization using multifractal detrended fluctuation analysis,” *Fluctuation Noise Lett.*, vol. 19, 2020, Art. no. 2050009.
- [25] G. F. Gu and W. X. Zhou, “Detrended fluctuation analysis for fractals and multifractals in higher dimensions,” *Phys. Rev. E*, vol. 74, no. 6, 2006, Art. no. 061104.
- [26] O. Velazquez-Camilo, E. Bolaños-Reynoso, E. Rodriguez, and J. Alvarez-Ramirez, “Fractal analysis of crystallization slurry images,” *J. Crystal Growth*, vol. 312, no. 6, pp. 842–850, 2010.
- [27] Q. Nie, J. Xu, W. Man, and F. Sun, “Detrended fluctuation analysis of spatial patterns on urban impervious surface,” *Environ. Earth Sci.*, vol. 74, no. 3, pp. 2531–2538, 2015.
- [28] R. P. Yadav, M. Kumar, A. K. Mittal, and A. C. Pandey, “Fractal and multifractal characteristics of swift heavy ion induced self-affine nanostructured BaF₂ thin film surfaces,” *Chaos, Interdisciplinary J. Nonlinear Sci.*, vol. 25, 2015, Art. no. 083115.
- [29] M. R. Niu *et al.*, “Multifractal detrended fluctuation analysis of combustion flames in four-burner impinging entrained-flow gasifier,” *Chem. Eng. J.*, vol. 143, no. 1/3, pp. 230–235, 2008.
- [30] C. Liu, X. L. Jiang, T. Liu, L. Zhao, W. X. Zhou, and W. K. Yuan, “Multifractal analysis of the fracture surfaces of foamed polypropylene/polyethylene blends,” *Appl. Surf. Sci.*, vol. 255, pp. 4239–4245, 2009.
- [31] R. P. Yadav, S. Dwivedi, A. K. Mittal, M. Kumar, and A. C. Pandey, “Fractal and multifractal analysis of LiF thin film surface,” *Appl. Surf. Sci.*, vol. 261, pp. 547–553, 2012.
- [32] G. Chander and B. Markham, “Revised Landsat-5 TM radiometric calibration procedures and postcalibration dynamic ranges,” *IEEE Trans. Geosci. Remote Sens.*, vol. 41, no. 11, pp. 2674–2677, Nov. 2003.
- [33] D. A. Artis and W. H. Carnahan, “Survey of emissivity variability in thermography of urban areas,” *Remote Sens. Environ.*, vol. 12, no. 4, pp. 313–329, 1982.
- [34] A. A. Van de Griend and M. Owe, “On the relationship between thermal emissivity and the normalized difference vegetation index for natural surfaces,” *Int. J. Remote Sens.*, vol. 14, pp. 1119–1131, 1993.
- [35] A. D. Gong, Z. X. Jiang, J. Li, Y. H. Chen, and H. L. Hu, “Urban land surface temperature retrieval based on Landsat TM remote sensing images in Beijing,” *Remote Sens. Inf.*, vol. 3, pp. 18–20, 2005.
- [36] T. C. Halsey, M. H. Jensen, L. P. Kadanoff, I. Procaccia, and B. I. Shraiman, “Fractal measures and their singularities: The characterization of strange sets,” *Phys. Rev. A*, vol. 33, no. 2, 1986, Art. no. 1141.
- [37] T. Lin, X. Xue, L. Shi, and L. Gao, “Urban spatial expansion and its impacts on island ecosystem services and landscape pattern: A case study of the island city of Xiamen, Southeast China,” *Ocean Coastal Manage.*, vol. 81, pp. 90–96, 2013.
- [38] L. Hua, J. Liao, H. Chen, D. Chen, and G. Shao, “Assessment of ecological risks induced by land use and land cover changes in Xiamen City, China,” *Int. J. Sustain. Develop. World Ecol.*, vol. 25, no. 5, pp. 439–447, 2018.
- [39] T. Lin *et al.*, “Spatial pattern of urban functional landscapes along an urban–rural gradient: A case study in Xiamen City, China,” *Int. J. Appl. Earth Observ. Geoinf.*, vol. 46, pp. 22–30, 2016.
- [40] W. Man, Q. Nie, Z. Li, H. Li, and X. Wu, “Using fractals and multifractals to characterize the spatiotemporal pattern of impervious surfaces in a coastal city: Xiamen, China,” *Phys. A, Statist. Mech. Appl.*, vol. 520, pp. 44–53, 2019.



QIN NIE received the Ph.D. degree in cartography and geography information system from the School of Geographic Sciences, East China Normal University, Shanghai, China, in 2013.

She is currently an Associate Professor with the Department of Spatial Information Science and Engineering, Xiamen University of Technology, Xiamen, China. Her major research interest includes remote sensing data mining, mostly fractal study on land surface temperature, and impervious surface.

KAI SHI received the Ph.D. degree in environmental sciences from the College of Architecture & Environment, Sichuan University, Chengdu, China, in 2008.

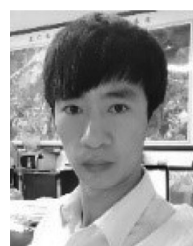
He is currently a Professor with the College of Biology and Environmental Sciences, Jishou University, Jishou, China, where he is also the Vice-Director of the Key Laboratory of Ecotourism in Hunan Province. His major research interest includes nonlinear analysis of complex environmental system.



YI GONG received the bachelor’s degree in information engineering from Wuhan University, Wuhan, China, in 2002, the M.A. degree in human geography from the University of Liverpool, Liverpool, U.K., in 2003, and the Ph.D. degree in human geography from University College London, London, U.K., in 2010.

She is currently a Research Fellow with the Sustainable Places Research Institute, Cardiff University, Cardiff, U.K. Her research interest focuses on how we can develop a better understanding of the interplay between the natural environment, built environment,

human behavior, and health.



FEIPENG RAN received the Ph.D. degree in cartography and geographic information engineering from the China University of Mining and Technology, Beijing, China, in 2015.

He is currently a Lecturer with the Department of Spatial Information Science and Engineering, Xiamen University of Technology, Xiamen, China. His research interests include 3-D GIS, 3-D panoramic geographic information systems, and geographic information system development.



Zongmei Li received the Ph.D. degree in cartography and geographic information system from the Institute of Remote Sensing and Digital Earth, Chinese Academy of Sciences, Beijing, China, in 2013.

She is currently an Associate Professor with the Department of Spatial Information Science and Engineering, Xiamen University of Technology, Xiamen, China. Her research interests include ecological remote sensing, landscape ecology, and climate change.

Lizhong Hua received the Ph.D. degree in physical geography from the Graduate School of the Chinese Academy of Sciences, Sichuan, China in 2007.

He is currently a Professor with the Department of Spatial Information Science and Engineering, Xiamen University of Technology, Xiamen, China. His research interests include urban ecology, urban heat island changes, and urban remote sensing application.

Runjing Chen received the Ph.D. degree in geodesy and survey engineering from the Institute of Geodesy and Geophysics, Chinese Academy of Sciences, Wuhan, China, in 2014.

He is currently a Lecturer with the Department of Surveying and Remote Sensing Engineering, Xiamen University of Technology, Xiamen, China. His research interest includes GNSS data processing and its applications in geodesy.